Sensors and Materials, Vol. 37, No. 8 (2025) 3651–3660
MYU Tokyo

S & M 4143

UV-C Light Detection in Aluminum Gallium Oxide Metal–Semiconductor–Metal Photodetectors

Tsung-I Liao,[1] Sheng-Po Chang,[2*] and Shoou-Jinn Chang[1,3]

[1]Program on Semiconductor Manufacturing Technology, Academy of Innovative Semiconductor and Sustainable Manufacturing, National Cheng Kung University, Tainan City 701, Taiwan
[2]Department of Microelectronics Engineering, National Kaohsiung University of Science and Technology, Kaohsiung City 811, Taiwan
[3]Institute of Microelectronics & Department of Electrical Engineering, National Cheng Kung University, Tainan City 701, Taiwan

(Received May 9, 2025; accepted August 4, 2025)

Keywords: transparent oxide semiconductors (TOSs), aluminum gallium oxide (AGO), UV photodetectors, co-sputtering

In this work, we fabricated aluminum gallium oxide (AGO) metal–semiconductor–metal photodetectors (PDs) with different RF powers of Ga_2O_3 target (P_{Ga}), and their characteristics were investigated and discussed. At P_{Ga} below 160 W, the PDs exhibited high resistance across the whole range of wavelengths. When P_{Ga} increases to 160 W or higher, both the response and rejection ratio improve significantly. The optimal photoresponse occurs when the DC power of Al is 80 W and P_{Ga} is 180 W, with the rejection ratio about 10^5, the responsivity 0.2 mA/W, the rise time less than 1 s, and the decay time less than 0.1 s. Additionally, the optimal AGO PDs have high stability and repeatability demonstrated in the time-resolved response.

1. Introduction

Transparent oxide semiconductors (TOSs) have attracted considerable attention owing to their wide range of applications, including but not limited to LEDs, liquid crystal displays, photosensors, and resistive random-access memory. The most used materials in TOSs include indium oxide,[1–3] gallium oxide (Ga_2O_3),[4–6] tin oxide,[7,8] zinc oxide,[9,10] indium gallium oxide,[11,12] indium tin oxide,[13,14] and indium gallium zinc oxide (IGZO).[15–18] These materials are well known for their excellent electrical conductivity, high optical transparency in the visible spectrum, and wide bandgaps.[19,20]

UV photodetectors (PDs) have attracted significant interest owing to their diverse applications in civilian infrastructure, military facilities, and optoelectronic circuits.[21,22] Additionally, UV PDs with a cut-off wavelength range from 200 to 280 nm are classified as solar-blind, as solar radiation in this range cannot penetrate Earth's atmosphere.[23] Therefore, solar-blind UV PDs with high stability offer various applications, such as UV leakage detection, biochemical sensing, and ozone depletion monitoring.[24]

*Corresponding author: e-mail: changsp@nkust.edu.tw
https://doi.org/10.18494/SAM5732

ISSN 0914-4935
https://myukk.org/

To enable UV detection, materials with wide bandgaps are preferred, as their large bandgap energies correspond to low cut-off wavelengths. As one of the wide-bandgap semiconductors, Ga_2O_3 is a good choice owing to its wide bandgap of 4.9–5.3 eV and high responsivity in the UV range.[25–28] However, Ga_2O_3 has a poor response to light below 250 nm.[29] Thus, Ga_2O_3-based compounds become a potential material. Therefore, we propose the use of aluminum gallium oxide (AGO) as a material to manufacture high-performance PDs for the UVC field, as it helps increase the bandgap. In this work, the fabrication of AGO UV PDs based on a metal–semiconductor–metal (MSM) structure was demonstrated. The effects of different Ga_2O_3 RF powers, optical characteristics, and electrical analysis were discussed. Focusing on solar-blind UV detection, we hope that the results of this study may provide a useful reference for the future research and development of high-performance UV PDs.

2. Experiment

First, 2 × 2 cm^2 quartz substrates were sequentially cleaned using acetone, isopropyl alcohol, and deionized water in an ultrasonic bath. Then, a 150-nm-thick AGO film was deposited in the same chamber by the co-sputtering method, where aluminum was sputtered using DC power and Ga_2O_3 was sputtered using RF power. While the DC power was fixed at 80 W, to modify the composition ratio, the RF power of the Ga_2O_3 target (P_{Ga}) varied from 100 to 200 W in 20 W increments. The chamber pressure was kept at 5 mTorr. The Ar and O_2 flow rates were set at 90 and 10 sccm, respectively. To fabricate MSM-structured PDs, Ni/Au interdigital electrodes of 30 nm/70 nm thickness were deposited on AGO films using an electron beam evaporator. The electrodes featured a finger width of 0.1 mm, a length of 1.2 mm, and a spacing of 0.2 mm between fingers, as depicted in Fig. 1. For the electrical characterization of the fabricated PD, we measured the light current, dark current, and time response using a semiconductor parameter analyzer (model B1500, Agilent Technologies) at room temperature and atmospheric pressure. The illumination system consisted of a 150 W Xe lamp and a monochromator, which provided a wavelength range of 200–800 nm. The power of the monochromator was measured using Nova II P/N7Z01550 power meters.

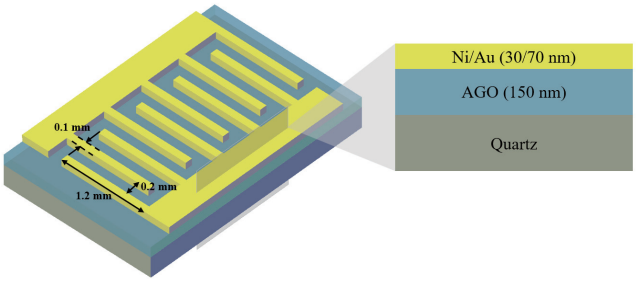

Fig. 1. (Color online) Schematic of AGO PD.

3. Results and Discussion

In Fig. 2(a), the transmittance spectra under different P_{Ga} values are shown. It can be observed that all the AGO films exhibit high optical transparency in the visible light band, with a transmittance rate of nearly 90%, and low transmittance in the ultraviolet region, particularly in the UVC range. The optical bandgap of AGO thin films can be determined using the Tauc relation as follows:[30,31]

$$(\alpha h\upsilon)^n = A\left(h\upsilon - E_g\right). \tag{1}$$

Figure 2(b) shows the Tauc plot derived from transmittance data. By extending the linear region of the curve to the *x*-axis, the optical energy gap of the film can be determined. Given that the energy gap of aluminum oxide is 6.3 eV and that of gallium oxide is 4.9 eV, an increase in P_{Ga} leads to a decrease in energy gap from 5.9 to 5.7 eV. As a result, the optical energy gap varies with different gallium oxide power levels. As P_{Ga} increases, the reduction in bandgap suggests that the physical properties of the AGO film become closer to those of Ga_2O_3. This implies that the electron affinity of the film shifts from that of Al_2O_3 (1.97 eV) toward that of Ga_2O_3 (4 eV). Consequently, not only does the bandgap of the AGO thin film slightly decrease, but the Schottky barrier between the metal and the AGO film also undergoes a significant reduction, leading to an increase in current once both a bias voltage and appropriate illumination with sufficiently high photon energy are applied. As a result, the corresponding photoresponse is expected to be enhanced. This suggests that if AGO MSM PDs are fabricated, they may exhibit improved performance owing to the reduced Schottky barrier.

To evaluate the UV photodetection capability of Ga_2O_3 films when co-sputtering AGO at different P_{Ga} values, we fabricated AGO MSM PDs as described above and measured their performance under specific conditions. The wavelength of the light source applied to devices

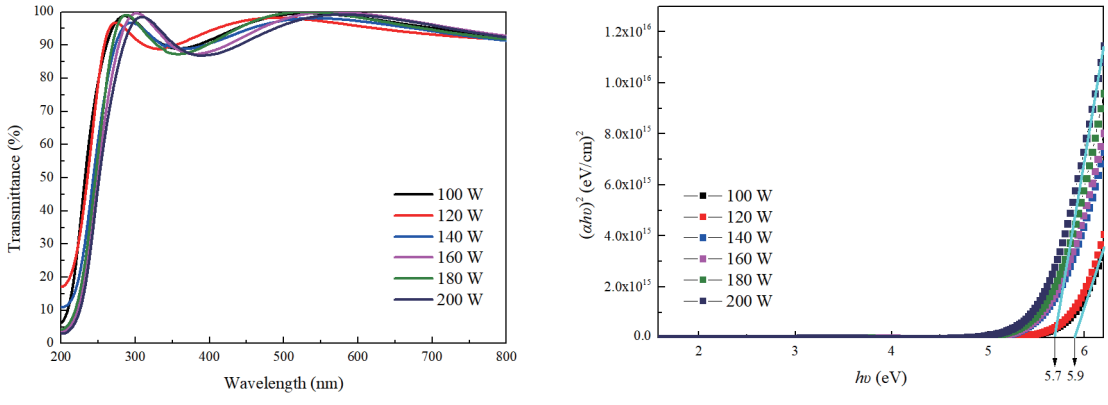

(a) (b)

Fig. 2. (Color online) (a) Transmittance spectra and (b) Tauc plot of AGO thin films with different Ga_2O_3 power levels.

ranges from 360 to 200 nm with 10 nm intervals and the bias applied to devices ranges from 0 to 10 V. The *I–V* characteristics of P_{Ga} ranging from 100 to 200 W are shown in Fig. 3. At lower P_{Ga} (100–140 W), although the films exhibit a photoresponse, the measured photocurrent-to-dark current ratio is less than 10, with most of the current being noise. Since the photocurrent above 250 nm is mostly noise, we only showed the response in the 200–250 nm range. As P_{Ga} increases to higher power levels (160–200 W), the dark current remains at 10^{-14} A, which is the

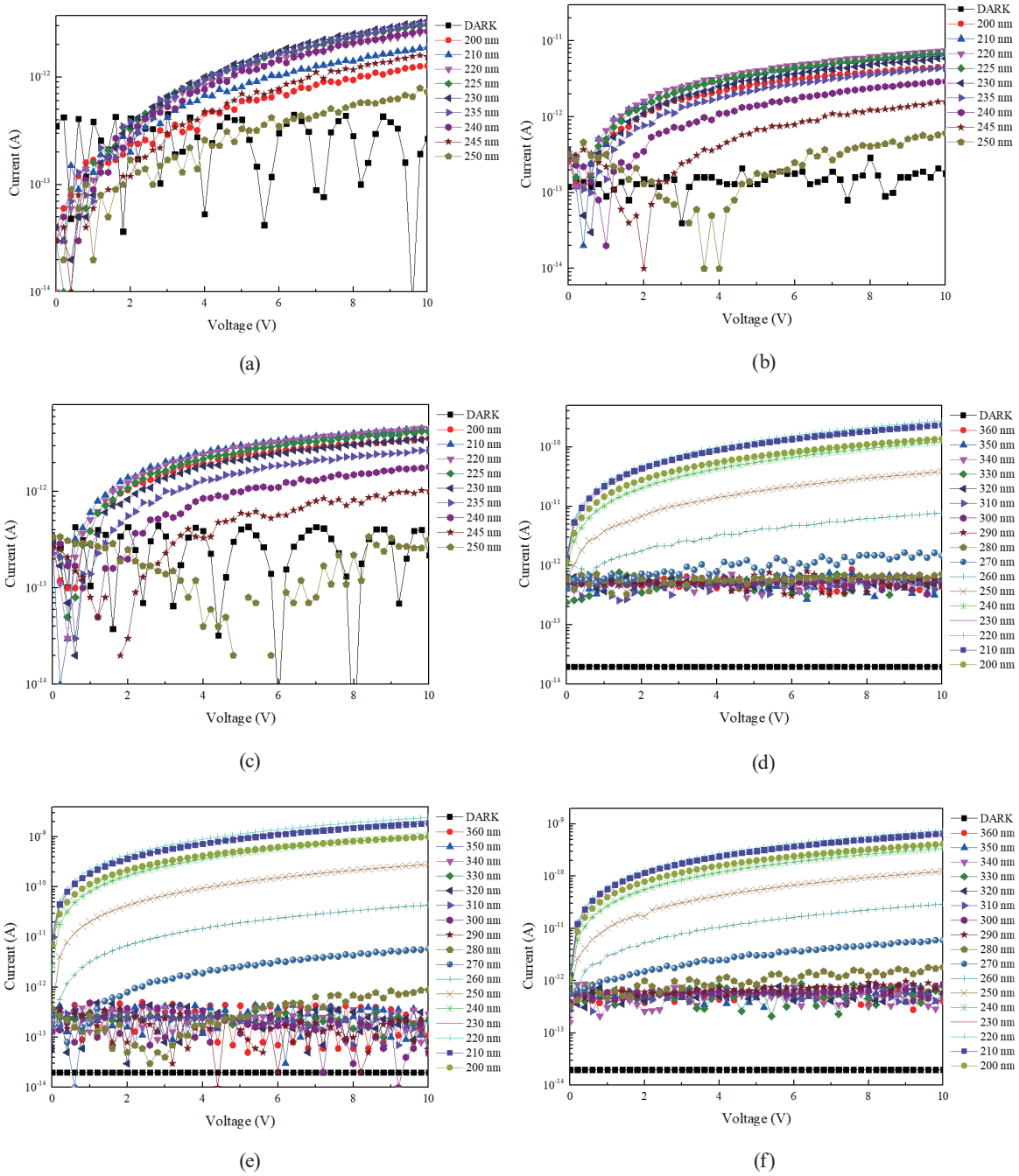

Fig. 3. (Color online) *I–V* curves under illumination of different wavelengths for AGO PD with Ga_2O_3 RF power ranging from 100 to 200 W. (a) 100, (b) 120, (c) 140, (d) 160, (e) 180, and (f) 200 W.

measurement limit of the equipment. Under light irradiation near 210 nm, the photocurrent is relatively significant, ranging from approximately 10^{-10} to 10^{-9} A.

The responsivity of AGO MSM PDs at low P_{Ga} values from 100 to 140 W, calculated from 200 to 250 nm in 10 nm intervals, is shown in Fig. 4(a). On the other hand, Fig. 4(b) shows the responsivity of AGO MSM PDs at high P_{Ga} values from 160 to 200 W, measured from 200 to 500 nm in 10 nm intervals. As P_{Ga} increases, the maximum responsivity increases from 0.02 to 0.2 mA/W under 210 nm light illumination. The rejection ratio (*RR*) reaches a maximum of 8.9×10^4 at 180 W. The *I*–*V* data, responsivity, and *RR* values for high P_{Ga} values are summarized in Table 1. In this work, we define *RR* as an indicator of UV wavelength selectivity. A higher *RR* indicates a higher UV selectivity in the deep-UV range. Specifically, *RR* is defined as the ratio of the responsivity at 210 nm to that at 300 nm and can be expressed as

$$RR = \frac{Responsivity(210\,\mathrm{nm})}{Responsivity(300\,\mathrm{nm})}. \tag{2}$$

A possible explanation for these results is that as P_{Ga} increases, the Schottky barrier between the metal and the AGO film undergoes a significant reduction. Although the peak responsivity occurs near 210 nm for all P_{Ga} values, this reduction facilitates the transport of photoexcited carriers, leading to a substantial photocurrent.[32] This effect is crucial for achieving a notable

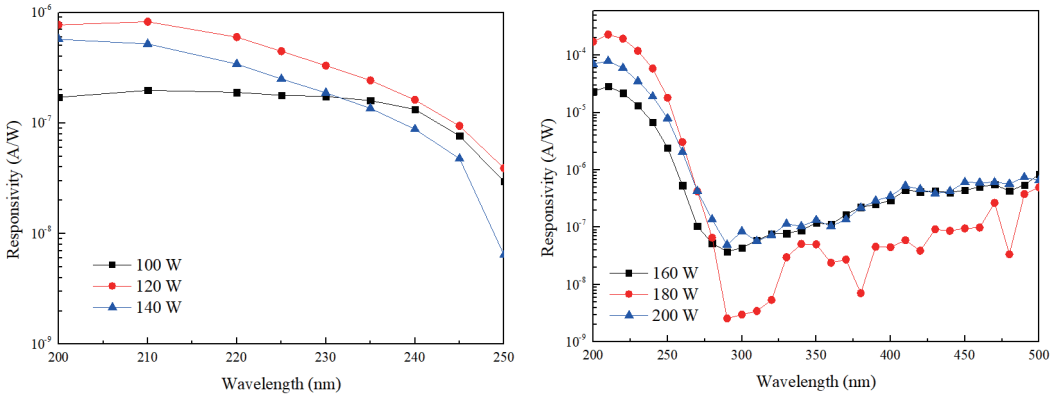

(a) (b)

Fig. 4. (Color online) Responsivity of different wavelengths of AGO MSM PDs with Ga_2O_3 RF powers ranging from (a) 100 to 140 W and (b) 160 to 200 W.

Table 1
Characteristics of AGO MSM PDs.

Ga_2O_3 RF power (W)	Photocurrent at 210 nm (A)	Photo/dark current ratio	Peak responsivity (A/W)	*RR*
100	3.19×10^{-12}	7.06	1.98×10^{-7}	—
120	6.99×10^{-12}	25.24	8.25×10^{-7}	—
140	4.50×10^{-12}	16.23	5.72×10^{-7}	—
160	2.38×10^{-10}	1.29×10^3	2.86×10^{-5}	7.59×10^2
180	1.88×10^{-9}	2.62×10^3	2.30×10^{-4}	8.95×10^4
200	9.95×10^{-10}	2.75×10^3	7.96×10^{-5}	1.60×10^3

RR. At P_{Ga} below 160 W, the photoexcited carriers cannot overcome the barrier, causing the PDs to exhibit high resistance across the whole range of wavelengths. However, when P_{Ga} reaches 160 W, photoexcited carriers begin to generate a more notable photocurrent. The optimal performance at 180 W results from a balance between carrier transport efficiency and Schottky barrier reduction. At higher P_{Ga}, excessive ion bombardment induces lattice strain, increasing defect density and phonon scattering, which reduces carrier mobility and makes it more difficult for photoexcited carriers to reach the electrodes, thereby lowering the photocurrent at 200 W.[33] Additionally, while increasing P_{Ga} reduces the Schottky barrier, excessive reduction at 200 W leads to a significant increase in dark current owing to thermionic emission or tunneling effects, decreasing the light-to-dark current ratio and weakening the overall photoresponse. At 180 W, these competing effects reach an optimal balance, where the barrier is sufficiently lowered to enhance carrier transport while lattice strain and dark current remain controlled, resulting in the highest responsivity and *RR*.

The time-resolved response of AGO MSM PDs is also discussed. Figures 5(a)–5(c) show the time response of PDs with P_{Ga} values ranging from 160 to 200 W, and the average response times are listed in Table 2. This power range demonstrates significantly enhanced responsivity,

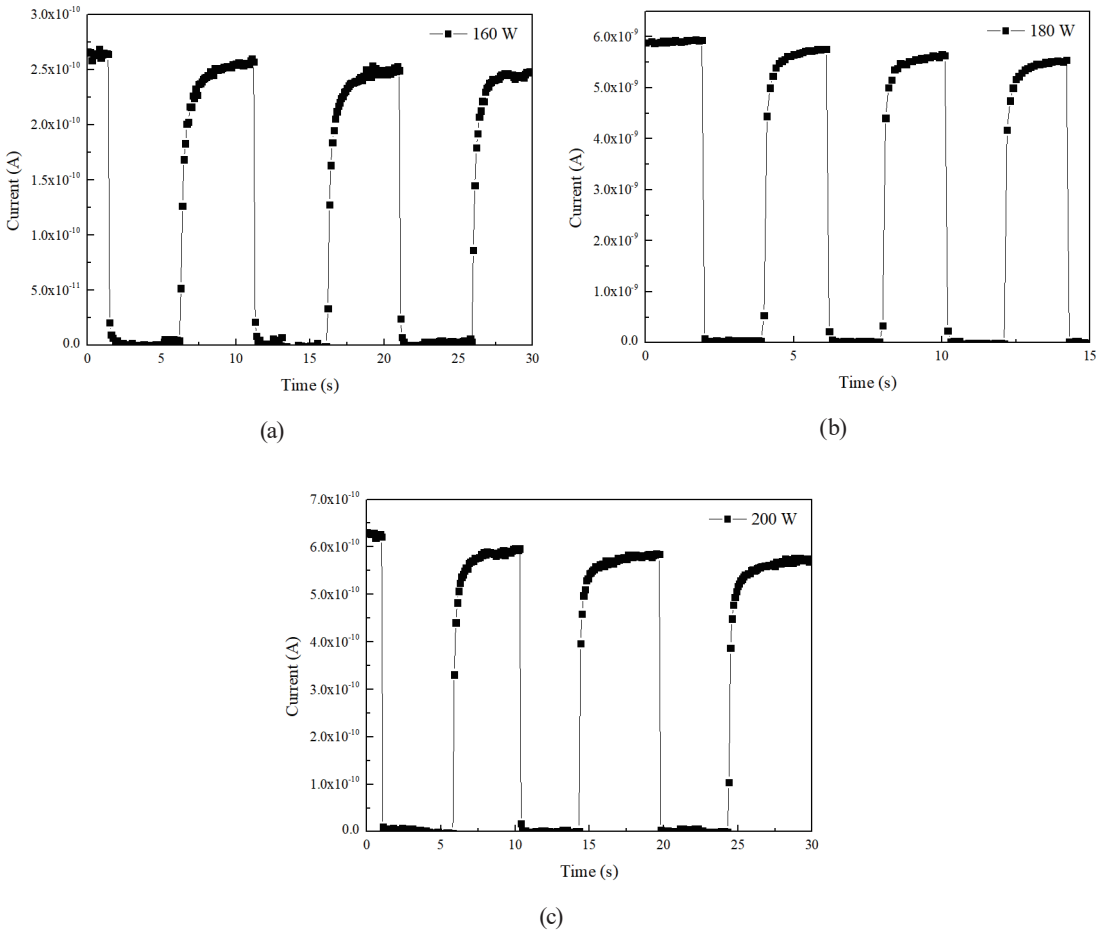

Fig. 5. Time-resolved response of AGO MSM PDs with Ga_2O_3 RF powers of (a) 160, (b) 180, and (c) 200 W.

Table 2
Average response time of AGO MSM PDs with high Ga_2O_3 RF powers.

Ga_2O_3 RF power (W)	Rising time (s)	Falling time (s)
160	1.55	0.04
180	0.51	0.06
200	1.16	0.08

Table 3
Performance comparison of solar-blind PDs with AGO.

Reference	Dark current (A)	Peak responsivity (A/W)	*RR*	Rising time (s)	Falling time (s)
This work	$\sim 10^{-14}$	2.30×10^{-4} @10 V, 210 nm	8.95×10^4	0.51	0.06
Ref. 36	$\sim 10^{-12}$	0.07 @5 V, 230 nm	1.54×10^3	—	—
Ref. 37	$\sim 10^{-12}$	0.50 @5 V, 240 nm	1.24×10^2	~2	~0.05
Ref. 38	$\sim 10^{-13}$	1.38 @5 V, 230 nm	—	~3	~0.30
Ref. 39	$\sim 10^{-12}$	0.50 @5 V, 240 nm	$\sim 10^3$	—	A few seconds

making it more suitable for time response measurements. The AGO PDs exhibit high stability and repeatability, with a rise time of less than 1 s and a fall time within 0.1 s. The rise time is defined as the duration required for the current to increase from 10 to 90% of the peak value under continuous illumination, whereas the fall time is the duration required for the current to decay from 90 to 10% when the light source is removed. The measurements were conducted under 210 nm illumination with a bias voltage of 10 V, and all devices were switched ON/OFF for three cycles. Notably, the fast-falling behavior suggests that the AGO PDs exhibit a minimal persistent photoconductivity (PPC) effect, which is commonly observed in IGZO-based PDs.[34,35] Although the exact mechanism is still under investigation, the reduced PPC observed in this study may be related to the improved film quality achieved through the current deposition process. A performance comparison of the solar-blind PDs with AGO is shown in Table 3. Compared with previous reports, our devices exhibit notably lower dark current, higher *RR*, and faster time response, demonstrating the improved performance achieved through our fabrication process and device design. Therefore, in this work, we not only demonstrate the viability of AGO for UVC detection but also highlight the importance of process optimization in achieving high-performance UV sensors.

4. Conclusions

The results demonstrated that the performance of AGO PDs varies with P_{Ga}. When P_{Ga} increases to 160 W or higher, both the response and *RR* improve significantly. This improvement can be explained by the Schottky barrier between the metal and the AGO film. As P_{Ga} increases, the barrier between gallium oxide and the metal decreases. With a smaller barrier, photoexcited carriers can generate a more significant photocurrent, leading to higher response and *RR*.

Our best-performing process parameters are obtained when the DC power of Al is 80 W, P_{Ga} is 180 W, and the argon/oxygen ratio is 90/10 sccm. Under these conditions, the peak wavelength is 210 nm, the responsivity is approximately 0.2 mA/W, *RR* is about 10^4, the responsivity is 0.2 mA/W, the rise time is less than 1 s, and the decay time is less than 0.1 s with high stability and repeatability.

Acknowledgments

This work was supported by the National Science and Technology Council under contract number NSTC 113-2221-E-992-110.

References

1 G. Cai, Z. Chen, L. Qiang, B. Yan, Y. Zhuo, J. Lin, X. Wang, Y. Pei, and G. Wang: Jpn. J. Appl. Phys. **57** (2018) 110301. https://doi.org/10.7567/JJAP.57.110301
2 H.-L. Zhao, F. Shan, X.-L. Wang, J.-Y. Lee, and S.-J. Kim: IEEE J. Electron Devices Soc. **10** (2022) 379. https://doi.org/10.1109/JEDS.2022.3170111
3 F. Shan, H.-Z. Sun, J.-Y. Lee, S. Pyo, and S.-J. Kim: IEEE Access **9** (2021) 44453. https://doi.org/10.1109/ACCESS.2021.3056774
4 M. I. Pintor-Monroy, M. G. Reyes-Banda, C. Avila-Avendano, and M. A. Quevedo-Lopez: IEEE Sens. J. **21** (2021) 14807. https://doi.org/10.1109/JSEN.2021.3074623
5 Y. Qin, L. H. Li, Z. Yu, F. Wu, D. Dong, W. Guo, Z. Zhang, J. H. Yuan, K. H. Xue, and X. Miao: Adv. Sci. **8** (2021) 2101106. https://doi.org/10.1002/advs.202101106
6 Y. Wang, H. Li, J. Cao, J. Shen, Q. Zhang, Y. Yang, Z. Dong, T. Zhou, Y. Zhang, and W. Tang: ACS Nano **15** (2021) 16654. https://doi.org/10.1021/acsnano.1c06567
7 J.-M. Wu and C.-H. Kuo: Thin solid films **517** (2009) 3870. https://doi.org/10.1016/j.tsf.2009.01.120
8 C. W. Shih, A. Chin, C. F. Lu, and W. F. Su: IEEE Electron Device Lett. **40** (2019) 909. https://doi.org/10.1109/LED.2019.2912032
9 D. A. Mourey, D. A. Zhao, and T. N. Jackson: IEEE Electron Device Lett. **31** (2010) 326. https://doi.org/10.1109/LED.2010.2041424
10 Y.-L. Chu, Y.-H. Liu, T.-T. Chu, and S.-J. Young: IEEE Sens. J. **22** (2022) 5644. https://doi.org/10.1109/JSEN.2022.3150254
11 T.-H. Chang, S.-J. Chang, W.-Y. Weng, C.-J. Chiu, and C.-Y. Wei: IEEE Photonics Technol. Lett. **27** (2015) 2083. https://doi.org/10.1109/LPT.2015.2453317
12 S.-P. Chang, L.-Y. Chang, and J.-Y. Li: Sensors **16** (2016) 2145. https://doi.org/10.3390/s16122145
13 X. Li, Z. Deng, J. Li, Y. Li, L. Guo, Y. Jiang, Z. Ma, L. Wang, C. Du, and Y. Wang: Photonics Res. **8** (2020) 1662. https://doi.org/10.1364/PRJ.398450
14 H. Ferhati and F. Djeffal: IEEE Sens. J. **19** (2019) 7942. https://doi.org/10.1109/JSEN.2019.2920815
15 Y. Han, J. Seo, D. H. Lee, and H. Yoo: Micromachines **16** (2025) 118. https://doi.org/10.3390/mi16020118
16 Y. Schellander, M. Winter, M. Schamber, F. Munkes, P. Schalberger, H. Kuebler, T. Pfau, and N. Fruehauf: J. Soc. Inf. Disp. **31** (2023) 363. https://doi.org/10.1002/jsid.1202
17 C. Chiu, W. Weng, S. Chang, S.-P. Chang, and T. Chang: IEEE Sens. J. **11** (2011) 2902. https://doi.org/10.1109/JSEN.2011.2146770
18 E.-G. Chong, Y.-S. Chun, S.-H. Kim, and S.-Y. Lee: J. Electr. Eng. Technol. **6** (2011) 539. https://doi.org/10.5370/JEET.2011.6.4.539
19 J. Shi, J. Zhang, L. Yang, M. Qu, D. C. Qi, and K. H. Zhang: Adv. Mater. **33** (2021) 2006230. https://doi.org/10.1002/adma.202006230
20 H. Hosono: Thin Solid Films **515** (2007) 6000. https://doi.org/10.1016/j.tsf.2006.12.125
21 M. Patel, H. S. Kim, and J. Kim: Adv. Electron. Mater. **1** (2015) 1500232. https://doi.org/10.1002/aelm.201500232
22 S. Nakano, N. Saito, K. Miura, T. Sakano, T. Ueda, K. Sugi, H. Yamaguchi, I. Amemiya, M. Hiramatsu, and A. Ishida: J. Soc. Inf. Disp. **20** (2012) 493. https://doi.org/10.1002/jsid.111
23 A. Webb: Solar ultra-violet radiation and vitamin D synthesis in man, University of Nottingham (1985).

24 L. Wang, S. Xu, J. Yang, H. Huang, Z. Huo, J. Li, X. Xu, F. Ren, Y. He, and Y. Ma: ACS Omega **9** (2024) 25429. https://doi.org/10.1021/acsomega.4c02897
25 S. Sun, C. Wang, S. Alghamdi, H. Zhou, Y. Hao, and J. Zhang: Adv. Electron. Mater. **11** (2025) 2300844. https://doi.org/10.1002/aelm.202300844
26 D. Pyngrope, M. Biswas, S. Kumar, S. Majumdar, and A. Bag: Mater. Sci. Semicond. Process. **174** (2024) 108243. https://doi.org/10.1016/j.mssp.2024.108243
27 Z. Liu, Y. Liu, X. Wang, W. Li, Y. Zhi, X. Wang, P. Li, and W. Tang: J. Appl. Phys. **126** (2019) 045707. https://doi.org/10.1063/1.5112067
28 X. Xiu, L. Zhang, Y. Li, Z. Xiong, R. Zhang, and Y. Zheng: J. Semicond. **40** (2019) 011805. https://doi.org/10.1088/1674-4926/40/1/011805
29 S. Cui, Z. Mei, Y. Zhang, H. Liang, and X. Du: Adv. Opt. Mater. **5** (2017) 1700454. https://doi.org/10.1002/adom.201700454
30 F. Shan, B. Shin, S. Jang, and Y. Yu: J. Eur. Ceram. Soc. **24** (2004) 1015. https://doi.org/10.1016/S0955-2219(03)00397-2
31 M. G. Yun, S. H. Kim, C. H. Ahn, S. W. Cho, and H. K. Cho: J. Phys. D: Appl. Phys. **46** (2013) 475106. https://doi.org/10.1088/0022-3727/46/47/475106
32 C.-N. Lin, Z.-F. Zhang, Y.-J. Lu, X. Yang, Y. Zhang, X. Li, J.-H. Zang, X.-C. Pang, L. Dong, and C. X. Shan: Carbon **200** (2022) 510. https://doi.org/10.1016/j.carbon.2022.09.001
33 P. Sharma, K. Sreenivas, and K. Rao: J. Appl. Phys. **93** (2003) 3963. https://doi.org/10.1063/1.1558994
34 J. T. Jang, D. Ko, S. Choi, H. Kang, J.-Y. Kim, H. R. Yu, G. Ahn, H. Jung, J. Rhee, and H. Lee: Solid-State Electron. **140** (2018) 115. https://doi.org/10.1016/j.sse.2017.10.028
35 J. Yu, K. Javaid, L. Liang, W. Wu, Y. Liang, A. Song, H. Zhang, W. Shi, T.-C. Chang, and H. Cao: ACS Appl. Mater. Interfaces **10** (2018) 8102. https://doi.org/10.1021/acsami.7b16498
36 H.-Y. Lee, J.-T. Liu, and C.-T. Lee: IEEE Photonics Technol. Lett. **30** (2018) 549. https://doi.org/10.1109/LPT.2018.2803763
37 S.-H. Yuan, S.-L. Ou, S.-Y. Huang, and D.-S. Wuu: ACS Appl. Mater. Interfaces **11** (2019) 17563. https://doi.org/10.1021/acsami.9b04354
38 S.-H. Yuan, C.-C. Wang, S.-Y. Huang, and D.-S. Wuu: IEEE Electron Device Lett. **39** (2017) 220. https://doi.org/10.1109/LED.2017.2782693
39 S.-H. Yuan, S.-L. Ou, C.-C. Wang, S.-Y. Huang, C.-M. Chen, K.-Y. Lin, Y.-A. Chen, and D.-S. Wuu: Jpn. J. Appl. Phys. **57** (2018) 070301. https://doi.org/10.7567/JJAP.57.070301

About the Authors

Tsung-I Liao received his B.S. degree from National Cheng Kung University, Taiwan (R.O.C.). He is now studying for his direct Ph.D. degree from the Academy of Innovative Semiconductor and Sustainable Manufacturing at the same university. His research interests are in GaN HEMT and GaN-based sensors.

Sheng-Po Chang received his B.S. degree in electronic engineering from Southern Taiwan University of Science and Technology, Tainan, Taiwan, in 2004, and his M.S. degree in nanotechnology and microsystems engineering and Ph.D. degree in microelectronics, both from National Cheng Kung University (NCKU), Tainan, in 2006 and 2009, respectively. He is currently an assistant professor with the Department of Microelectronics Engineering, National Kaohsiung University of Science and Technology. His current research interests include II–VI and III–V optoelectronic devices, semiconductor physics, solar cells, and nanotechnology.

Shoou-Jinn Chang received his B.S. degree from National Cheng Kung University (NCKU), Tainan, Taiwan, in 1983, his M.S. degree from the State University of New York, Stony Brook, NY, USA, in 1985, and his Ph.D. degree from the University of California, Los Angeles, CA, USA, in 1989, all in electrical engineering. From 1989 to 1992, he was a research scientist with Nippon Telegraph and Telephone Basic Research Laboratories, Musashino, Tokyo, Japan. He joined the Department of Electrical Engineering, NCKU, in 1992 as an associate professor, where he was promoted to full professor in 1998. He served as the Director of the Institute of Microelectronics, NCKU from August 2008 to July 2011, and the Deputy Director of the Center for Micro/Nano Science and Technology, NCKU from February 2006 to January 2011. He is currently the Deputy Director of the Advanced Optoelectronic Technology Center, NCKU. From January to March 1999, he was a Royal Society Visiting Scholar with the University of Wales, Swansea, U.K.; from July 1999 to February 2000, he was a Visiting Scholar with the Research Center for Advanced Science and Technology, University of Tokyo, Tokyo, Japan; from August to September 2001, he was a Visiting Scholar with the Institute of Microstructural Science, National Research Council, Canada; from August to September 2002, he was a Visiting Scholar with the Institute of Physics, Stuttgart University, Stuttgart, Germany; and from July to September 2005, he was a Visiting Scholar with the Faculty of Engineering, Waseda University, Tokyo. He is also an Honorary Professor of Changchun University of Science and Technology, China. His current research interests include semiconductor physics, optoelectronic devices, and nanotechnology. Dr. Chang received the Outstanding Research Award from the National Science Council, Taiwan, in 2004. He is a Fellow of the Optical Society of America (OSA), the International Society for Optical Engineers (SPIE), and the Institute of Electrical and Electronics Engineers (IEEE).